Integrated convolutional neural network for skin cancer classification by hair and noise restoration

Nidhi BANSAL [1,*], Sridhar PANNEERSELVAM [2]

[1] Department of Information Science and Technology, CEG, Anna University, Chennai, Tamil Nadu, India

[2] Department of Information Science and Technology, CEG, Anna University, Chennai, Tamil Nadu, India

***Correspondence:** Nidhibansal.prof@outlook.com

ORCIDs:

Nidhi BANSAL: https://orcid.org/0009-0003-4387-7857

Sridhar PANNEERSELVAM: https://orcid.org/0009-0004-6349-5562

Abstract

Background/Aim: Skin lesions are commonly diagnosed and classified using dermoscopic images. There are many artefacts visible in dermoscopy images, including hair strands, noise, bubbles, blood vessels, poor illumination, and moles. As a result, these artefacts can obscure crucial information about lesions, which limits the ability to diagnose lesions automatically.

Materials and methods: In this work, it is investigated how hair and noise artefacts in lesion images affect classifier performance and how they can be removed to improve diagnostic accuracy. A synthetic dataset created using hair simulation and noise simulation is used in conjunction with the HAM10000 benchmark dataset. Moreover, an integrated Convolutional Neural Network (CNN) has been proposed individually for (i) removing hair artefacts using hair inpainting and classification of refined dehair images called Integrated Hair Removal (IHR), (ii) removing noise artefacts using non-local mean denoising and classification of refined denoised images called Integrated Noise Removal (INR).

Results: Five deep learning models are used for the classification: ResNet50, DenseNet121, ResNet152, VGG16, and VGG19. The proposed IHR-DenseNet121, IHR-ResNet50, and IHR-ResNet152 achieve 2.3%, 1.78%, and 1.89% higher accuracy than DenseNet121, ResNet50, and ResNet152 respectively by removing hairs. The proposed INR-DenseNet121, INR-ResNet50, and INR-VGG19 achieve 1.41%, 2.39%, and 18.4% higher accuracy than DenseNet121, ResNet50, and VGG19 respectively by removing noise.

Conclusion: A significant proportion of pixels within the lesion area are influenced by hair and noise, resulting in reduced classification accuracy. However, the proposed CNNs based on Image Hair Restoration (IHR) and Image Noise Reduction (INR) exhibit notably improved performance when restoring pixels affected by hair and noise. The performance outcomes of this proposed approach surpass those of existing methods.

Keywords: Dermoscopic images, image hair, image noise, convolutional neural network, image restoration, classification

1. Introduction

Skin cancer is the most prevalent type of cancer, accounting for millions of fatalities worldwide. Melanoma is the deadliest form of skin cancer, causing 10,000 deaths worldwide [1]. Melanoma incidence has increased rapidly all over the world during the last fifty years [2]. The survival rate is over 95% if detected early and only about 15% for late survival [3]. This huge difference emphasizes the importance of melanoma detection and diagnosis at an early stage because it is treatable at this time. Timely detection helps in reducing mortality rates and hence preserves patient lives. Dermoscopy is an imaging procedure that aids in the analysis of skin lesions [4]. The sub-surface structures of the skin can be visually enhanced, exposing deeper skin lesions [5] and providing higher accuracy than the naked eye assessment. However, manual diagnosis demands an expert dermatologist and also suffers from subjective variation and clinical experience, lowering the patient's life expectancy [6]. As a result, computer-aided diagnosis (CAD) systems have emerged to help improve the efficiency of dermoscopy image analysis [7]. An accurate automatic melanoma diagnostic system is critical to assisting dermatologists in making precise diagnosis decisions and reducing the number of unnecessary biopsies. In the arena of clinical medicine, deep neural networks (DNNs) have made major progress and achieved excellent results in image segmentation and classification tasks [8]. However, accurate recognition of skin lesions from dermoscopic images is challenging owing to the presence of certain artefacts, including hair strands, noise, air bubbles, blood vessels, clinical marks, uneven lighting, etc. Skin lesions may be partly obscured or covered by these artefacts, creating a partial occlusion. This kind of image with a partly obscured region makes the diagnosis of an infected area extremely difficult [9].

Many classical techniques have been used in literature for hair and noise removal in dermoscopic images [10-18]. Lee et al. [10] presented the first method to remove thick hairs called Dull Razor and used bilinear interpolation. The PDE-based continuous morphological filter has been used by D H Chung et al. to remove undesirable hairs [11]. Curvilinear analysis has been used by Zhou et al. to achieve automatic hair and ruler marking recognition, and the artefact is replaced with a feature-guided exemplar-based inpainting technique [12]. To eliminate features from dark hair, Silveira invented the morphological closing and median filter [13]. Top hat filtering is applied by Xie to eradicate thin and curled hairs followed by PDE base inpainting [14]. Abbas et al. [2011] introduced a hair detection and repairing algorithm by using a derivative of Gaussian method to remove hair and then inpaint using a fast-marching method [15]. Toossi et al. [16] implemented a canny edge detector and morphological operators to segment hairs and ruler markings. Multi-resolution transport inpainting is applied to repair hair. Abuzaghleh et al. [17] proposed 84 directional filters to identify and disregard hair in skin lesions. Reda Kasmi et al. offered a new method by using 11×11 median filters to remove thin hairs and a Gabor filter for thick hairs [18]. There are some existing methods for noise removal in images [19-25]. A new method for Gaussian noise removal is proposed using multiscale filter banks [20]. A novel effective noise estimation method is proposed based on singular values of corrupted images [21].

A few deep learning methods are available for hair removal and image denoising tasks [26-30]. A CNN is built with a post-processing step using the Savitzky-Golay filter and Fourier Domain Filtering [26]. This method can detect the borders belonging to the hair follicles with an average Dice score of 0.83 ± 0.06. A FCN8-ResNetC based approach for hair removal and segmentation in dermoscopic images is proposed, the training accuracy obtained is 89.38% for hair removal [27]. Jain et al. [28] proposed a fully convolutional CNN for image denoising. An image denoising and blind inpainting method is proposed to combine sparse coding with pre-trained CNNs, achieving decent results in both tasks [29]. Mao et al. proposed an encoding-decoding framework for image denoising and super-resolution. The method combines convolution and deconvolution layers symmetrically by skip connections, which improves the network's performance [30].

The limitations of existing research are 1) The present research works mainly measured the hair detection accuracy and error, completely oblivious to the impact on skin lesion patterns. 2) Despite the availability of several methods for hair and noise removal, none of the works focus on the impact of eliminating these artefacts on the overall performance of a CAD system. It is essential to address the effects of hair lines and image noise on the classification accuracy of dermoscopic images to achieve better results and treatment. A deep learning model is developed for the removal of these artefacts. This model could be built into a complete CAD system for dermoscopic images. In this paper, it is studied how the hair and noise data overall affect the automatic detection of skin lesions. The deep learning model is run with the hair and noise artefacts and compared with ground truth images. An Integrated Convolutional Neural Network (CNN) with image inpainting is proposed to fix unwanted hairs and restore the color and texture of skin pixels below them (called dehairing), termed Integrated Hair Removal (IHR). This network performs image inpainting to eliminate unwanted hair initially and then integrates with deep learning models to perform classification and study the effect of removing hair. Secondly, an Integrated CNN with image denoising is implemented to remove noise from images (called denoising), termed Integrated Noise removal (INR). This integrated CNN first performs image denoising to reduce noise and then integrates with deep learning models to perform classification and study the effect of removing noise. The training and validation results after dehairing and denoising are compared with ground truth images. The results show that the training and validation accuracies improve when hair strands and noise are eliminated. These artefacts removal helps in better pattern analysis of dermoscopy images by de-occluding lesion boundary or texture, hence resulting in accurate classification. The core contributions of the work are:

- The investigation of the effect of image distortions like hair and noise on the performance of a skin CAD system.
- Two datasets are created wherein new hairs and noise are added.
- Integrated CNNs namely IHR and INR are developed to leverage the advantage of removing hair and noise artefacts integrated with deep learning models for the improved classification of skin lesions.
- The evaluation of the performance of proposed integrated deep learning models against the hairy and noisy dataset through extensive experimentation.
- Assessing the improved results based on accuracy and loss function when these distortions are removed.

The remainder of the paper is structured as: Section 2 covers the dataset used, proposed methodology, architecture, and network training. Section 3 presents the implementation and experimental results. In Section 4 results are discussed to analyze the performance of the proposed work. Section 5 includes the conclusion and future aspects of the work.

2. Materials and Method

2.1. Dataset Description

The benchmark dataset HAM10000 [31] is considered in this work. This is the ISBI Challenge dataset available as ISIC 2018. It is a collection of 10015 skin lesion images divided into seven categories. The seven classes are melanocytic nevus, basal cell carcinoma, actinic keratosis, melanoma, benign keratosis, dermatofibroma, and vascular lesion.

In a real-life scenario, the major artefacts causing factors are hair and noise. Though the images in the dataset are partially occluded by artefacts namely hair, rulers, moles, ink markings, etc. there are very few images causing major occlusion. The major concern in the detection and assessment of lesions is the lack of an appropriate dataset with major artefacts like hair and noise. Therefore, two synthetic datasets are generated called Hair Dataset and Noise Dataset. The hair and noise are introduced in images to obstruct the lesion region. These datasets are created to produce partial occlusion in skin cancer images and contain 5000 images. The images in the Hair Dataset are occluded by adding hair strands. For the Noise Dataset, Gaussian noise [32] is added to create a partial occlusion of the lesion area. For training, 80% of the whole data is taken and for testing 20% data is considered. Table 1 shows images in each dataset.

Hair Dataset: Hair is a major partial occlusion causing element in dermoscopic images of skin. The skin images contain thick and thin hairlines. The 5000 images are chosen from the original HAM10000 dataset. These images chosen contain no hair or very few hairs. Hair is extracted from other dermoscopic images with more hair. This is done to maintain a natural hair artefact appearance. Hair is taken out from hairy images using masking technique and then these hairs are superimposed on selected images for Hair Dataset.

Noise Dataset: The 5000 images are chosen from the original HAM10000 dataset and noise is added. These images are chosen from the dataset that contains no noise. Low lighting and a scarcity of resources for capturing medical images with clinical equipment result in large noise fluctuations in lesion images. Gaussian noise [32] is opted here as it is a main source of noise in digital photos while acquisition, such as sensor noise brought on by inadequate lighting and transmission noise.

A (typically) modest amount will be added or subtracted from each pixel's original value in the image. In dermoscopic images, Gaussian noise is a major noise that can happen during acquisition. All images may contain noise, varying in intensity. Here, Gaussian noise is added with zero mean and scale (σ) varied from 1 to 30. Figure. 1(a-h) shows a few examples of Gaussian Noise added to Noise Dataset.

2.2. Proposed Methodology

The proposed Integrated CNN model is described in this section. The methods employed for hair and noise restoration i.e. IHR and INR are presented. The deep learning models used for dermoscopic images and their classification is discussed.

Convolutional Neural Networks

Convolutional neural networks (CNN) contribute to image and video recognition tasks on a broad scale. There are several advantages to employing CNN over standard neural networks, including the ability to learn spatial hierarchies of patterns. It enables CNN to acquire increasingly complex and abstract visual concepts and analyse images with great efficiency. A vast number of images are necessary to train a new CNN model. This scenario relates to a situation in which the entire network must be trained. In this situation, all the network's parameters must be learned from the ground up. This approach necessitates extremely large datasets, which are frequently unavailable for medical purposes. However, employing a standard network allows for the option of transfer learning.

Transfer learning is a technique that uses a model trained on one dataset as the basis for a model trained on another. The model that is already trained is known as a pre-trained model. Typically, these models are built on ImageNet [33], a dataset of over fourteen million images and can classify images into over 1,000 different categories. In addition to using the same architecture as a standard network, one may also use parameters learnt by the CNNs with earlier training on a different dataset. Therefore, to adjust the network for the classification of a new target dataset, there are two possible ways. One way is to replace only the final classification layer according to one's target dataset, i.e., the network can be used to classify new dataset images. In another approach, the parameters gained from the model's training over a large dataset are fine-tuned through transfer learning. This allows the network's early layers to extract highly generalizable patterns from a larger dataset, and the network's later layers will take on the details of the new dataset for the adapted model.

In this paper, the first approach is followed i.e., the final classification layer is modified. The proposed CNN for dermoscopic image classification is given in Figure. 2. As a result, the time-consuming training stages are avoided and benefits are gained from the features learnt during the training over many images through transfer learning.

The most successful methods submitted for ISIC challenges 2016, 2017, 2018, 2019 and 2020 [34] used CNNs pre-trained on the ImageNet [33] database. Five deep transfer learning models used in this work are ResNet50 [35], DenseNet121 [36], ResNet152 [35], VGG16 [37], and VGG19 [38]. These models are used to find how the system performs in the case of partly occluded image data. Table 2 shows the deep learning architectures used.

Integrated CNN with Image Inpainting for Hair Removal (Dehairing)

An integrated CNN with inpainting is proposed for the classification of dermoscopic images shown in Figure. 3. Integration here defines a combination of two methods viz. skin cancer image inpainting and classification. Inpainting is done to restore hairs by substituting them with patches that resemble the nearby pixels. This reduces the impact of hairs on diagnosis analysis. Five deep learning models are applied for the classification of refined skin cancer images. These models are named IHR-ResNet50, IHR-DenseNet121, IHR-ResNet152, IHR-VGG16, and IHR-VGG19. Algorithm 3 explains an integrated CNN with inpainting for hair removal. Hair Dataset contains 5000 images where new hairs are added (Ref. Section 2.1). Removal of dark, dense hairs and regions that resemble hair is to be done properly as it aids in effective segmentation and classification of features. Numerous techniques are available in the literature for removing hair in dermoscopic images, based on morphological operations [39] and thresholding [40]. Although being fast, these techniques tend to eliminate subtle, significant features that can be mistaken for hair. An effective method for dermoscopic hair removal is the black-hat transform followed by inpainting, which is employed here, and described in Algorithm 2.

The first step is to perform the Gaussian blur and median blur operations before applying other methods to reduce the high-frequency data. It removes noise and edges from an image while preserving its original data. Gaussian blur is a low-pass filter that determines the variation to apply to each pixel of the image using a Gaussian function. Its purpose is to smooth down sphere edges, which frequently have inconsistencies because of the marker's rough surface. It is also used to reduce skin lines, air bubbles, light, and small hairs around the lesion. The kernel used is 3* 3 and σ is the standard deviation of the Gaussian kernel. The median filter is a nonlinear filter and is very effective in removing noise while preserving edges. The current pixel value is replaced with the median value in a 3 x 3 neighborhood.

The input dermoscopic image is converted from RGB to grayscale, followed by a morphological filter to find the hair contours. The morphological filter, called "black hat," is employed on the grayscale image. It gives a difference between the closing and the given input image. Closing eliminates the foreground's tiny holes. Black Hat extracts the dark objects smaller than the structuring element and finally outputs them as bright spots. An 11 × 11 cross-shaped structural element is defined. To intensify the hair contours, a thresholding operation is applied to the output of the black hat filter. This generates a binary mask. All unrequired objects present in the dermoscopic image are discarded, and only the hairlines are detected. Following this, an inpainting algorithm, TELEA [41], given in Algorithm 1, is used to restore the image by removing the hair structures from it. It preserves the appearance by replacing the hair structures with nearby pixels, producing a clear dermoscopic image. The eq. (1) shows point p is inpainted as a function of all points q in $B_{\mathcal{E}}(p)$ by summing the estimates of all points q, weighted by a normalized weighting function w (p, q),

$$I(p) = \frac{\sum_{q \in B_{\mathcal{E}}(p)} w(p,q)[I(q) + \nabla I(q)(p-q)]}{\sum_{q \in B_{\mathcal{E}}(p)} w(p,q)} \quad (1)$$

where *I(q)* is the original image and *I(p)* is an inpainted image. In algorithm 1, Ω is the region to be inpainted, ∂Ω is the boundary of the region to be inpainted and $B_{\mathcal{E}}(p)$ is a neighborhood of p. To inpaint the whole Ω, apply Equation 1 iteratively to all the pixels of ∂Ω, in increasing distance from ∂Ω's initial position ∂Ωi. Complete the boundary inside Ω until the whole region has been inpainted. Figure. 4 shows the stages of the hair removal process.

Algorithm 1: INPAINT_TELEA

δΩi = boundary of the region to inpaint

δΩ = δΩi

while (δΩ not empty)

{

p = pixel of δΩ closest to δΩi

inpaint p using Eq.1

advance δΩ into Ω

}

Algorithm 2: Dehair_Inpainted (Image, Kernel, Mask)

Input: Image, Kernel, Mask

Output: Skin images with Inpainted Hair

G_Blur ⟵ GaussianBlur (Image, Kernel * Kernel, σ)

Med_blur ⟵ MedianBlur (G_Blur, Kernel)

Image_GrayScale ⟵ Color (Med_blur, RGB2GRAY)

Kernel1 ⟵ StructuringElement (Morph_Cross, Kernel)

Blackhat ⟵ MorphologyEx (Image_GrayScale, MORPH_BLACKHAT, Kernel1)

ret_v, Thresh2_Image ⟵ Threshold (Blackhat, Thresh, Thresh_MaxVal, THRESH_BINARY)

Output_Image ⟵ Inpaint (Med_blur, Thresh2_Image, 1, INPAINT_TELEA)

Dehair_Inpainted ⟵ Color (Output_Image, COLOR_BGR2RGB)

Algorithm 3: Integrated CNN with Inpainting for Hair Removal

Input: Skin Images from HAM10000

Output: Hair removal Inpainted results with Accuracy and Loss

1) Input Skin cancer Images M_1……. M_n

2) For each Image M_i,
   do
   Dehair_Inpainted (M_i, Kernel, Mask)
3) For each Dehair_Inpainted image M_i, resize = 224*224
4) Fine-tune the last fully connected (FC) layer of deep CNN to identify the probabilities of seven skin cancer classes.
5) Train five deep CNNs IHR-ResNet50, IHR-DenseNet121, IHR-ResNet152, IHR-VGG16 and IHR-VGG19.
6) Validate the model and calculate training and validation accuracy and loss for performance evaluation.

Integrated CNN with Image Denoising for Noise Removal (Denoising)

An integrated CNN with noise removal is proposed for the classification of dermoscopic images shown in Figure. 5. Integration here defines a combination of two methods viz. skin cancer images' noise removal and classification. Denoising is done to take out undesirable noise from images so that they can be better analyzed. Five deep learning models are applied for the classification of refined skin cancer images. These models are named INR-ResNet50, INR-DenseNet121, INR-ResNet152, INR-VGG16, and INR-VGG19. Algorithm 4 explains an integrated CNN with denoising for noise removal. 5000 images from the Noise Dataset, in which noise is added are now denoised. The process of reconstructing a signal from noisy images is referred to as denoising an image. Non-local means [42] is utilized as the method of denoising to remove any probable aberrations from the image. The Non-Local (NL) Means Algorithm selects a pixel, draws a small window around it, and searches the image for other windows of the same size. It then performs an average of all the windows and calculates the resultant value for the pixel. The non-local signifies the whole image search, not an individual region. Given a noisy image $v = \{v(i) \mid i \in I\}$, the $NL[v](i)$, for a pixel i, is computed as a weighted average of all the pixels in the image, given in Eq. (2),

$$NL[v](i) = \sum_{j \in I} w(i,j)v(j) \tag{2}$$

where $\{w(i, j)\}_j$ depends on the similarity between the pixels i and j. It is used as the OpenCV function: fastNlMeansDenoisingColored. The function converts the image to CIELAB color space and then separately denoises the L and AB components with given h parameters using the FastNon-LocalMeansDenoising function. Larger search windows require longer denoising times. The ideal value for the luminance and color components is 10, and the higher the value, the smoother the image will be. All the images from the Noise Dataset are run through this process for reconstruction.

Algorithm 4: Integrated CNN with Non-Local Means for Denoising

---

Input: Skin Images from HAM10000

Output: Noise removal results with Accuracy and Loss

1) Input Skin cancer Images M_1……..Mn
2) For each Image M_i,
   Denoise $\leftarrow$ fastNlMeansDenoisingColored (Input_img, Out_Image, Lum_comp, color_comp, template_win, search_win)
3) For each Denoised image M_i, resize = 224*224
4) Fine-tune the last fully connected (FC) layer of deep CNN to identify the probabilities of skin cancer classes.
5) Train five deep CNNs INR-ResNet50, INR-DenseNet121, INR-ResNet152, INR-VGG16 and INR-VGG19.
6) Validate the model and calculate training and validation accuracy and loss for performance evaluation.

2.3. Model Training

Transfer learning is employed for training the IHR and INR models on the dataset, utilizing pre-trained weights obtained through training on the ImageNet dataset. Five pre-trained models are implemented for the given dataset. The model's weights are loaded and the final fully connected layer is removed. The remaining part of the model is used as a feature extractor for the given dataset. A new final fully connected layer is added to get the skin lesion classes required for output which is 7.

The network is trained for 25 epochs. Table 1 shows the hyperparameters used to train the model. The input image size for the model is a 224 × 224 × 3 RGB image. ReLU [43] activation function is employed throughout the architecture and the optimization function used is Adam [44]. The loss function applied is categorical cross entropy [45]. Table 3 shows all the hyperparameters and their values.

Fully Connected Layer:

- There is a need to categorise the data into several classes after feature extraction, which can be achieved with a fully connected (FC) layer.
- The fully connected layer in the convolutional network takes the outcome of the convolution/pooling process and makes a classification judgement.
- *Fully Connected Input*: The output of the final Pooling/Convolutional Layer is flattened, turned into a single vector and sent as the input into the fully connected layer.
- *Fully Connected Output*: It gives the final probabilities for each label.
- The final layer employs the softmax activation function to determine the likelihood that the input belongs to one of several classes (classification). The class probabilities are calculated and output in a 3D array with [1 x 1 x N] dimensions, where N is the number of classes.

ReLU Activation Function:

- The rectified linear activation function (ReLU) [43] is a non-linear function and can learn complex relationships from the training data.
- ReLU is very easy to compute and implement since it just requires a comparison between its input and the value 0.
- A ReLU function will apply a max (0, x) function. The function outputs the input directly if it is positive, otherwise, it will output zero.
- Derivative remains constant i.e. 1 for a positive input and thus reduces the time taken for the model to learn and in minimizing the errors.
- ReLU has a predictable gradient for the backpropagation of the error. As a consequence, the computation speed is very quick.

Categorical Cross-Entropy Loss:

- The network's performance is measured using a metric (loss function) that counts the similarity between predicted and actual value. Cross-entropy loss is the most important cost function used in multi-class classification.
- The objective of the loss function is to optimize the model during training [45]. To optimise the loss function, parameters are modified iteratively and help in correct prediction.
- The model performs better when loss is low.

3. Experimental Results and Discussion

The implementation of the proposed architecture is done in Google Colab. The classification accuracy and loss of the trained CNN models are calculated for training and validation. ResNet50 [35], DenseNet121 [36], ResNet152 [35], VGG16 [37], and VGG19 [38] models are run on ground truth images from HAM10000 Dataset and the corresponding images adulterated by the Hair Dataset and Noise Dataset. The models IHR-ResNet50, IHR-DenseNet121, IHR-ResNet152, IHR-VGG16, and IHR-VGG19 are run on Hair Dataset after dehairing. The models INR-ResNet50, INR-DenseNet121, INR- ResNet152, INR-VGG16, and INR-VGG19 are run on Noise Dataset after denoising the images. All the models are run for 25 epochs. Here, the results are shown after 10, 15, and 25 epochs. The performance metrics used to validate the results are Training Accuracy (TAcc), Training Loss (TLoss), Validation Accuracy (VAcc), and Validation Loss (VLoss).

3.1. Experimental Results on HAM Dataset

Skin cancer images are taken from the Ground Truth (GT) Dataset (HAM). This dataset comprises 10,015 images. All the models are run on these images. Table 4 shows training and validation accuracies on the GT Dataset. Table 5 shows training and validation loss on the GT Dataset.

3.2. Experimental Results with Hair Dataset

The model performance for Hair Dataset is shown in Tables 6-9. Table 6 shows training and validation accuracy on Hair Occluded images. Table 7 shows training and validation loss on Hair Occluded images. DenseNet121 gives a training accuracy of 95.20% with a validation accuracy of 87.10%. VGG19 with occluded hair gives a training accuracy of 85.03 and a validation accuracy of 78.62%.

Dehairing results using Proposed Integrated CNN with Hair Inpainting

Dehairing is performed using Algorithm 3 proposed in Section 2.2. Table 8 shows training and validation accuracy after Dehairing. Table 9 shows training and validation loss after Dehairing. It can be seen that training and validation accuracy decreases when the skin image is occluded with hair strands. DenseNet121 gives a training accuracy of 95.20%

with hair while IHR-DenseNet121 provides 97.50% accuracy with hair removal. The validation accuracy with Densenet121 is 87.10% when hair is present while 89.16% with IHR-DenseNet121 when hairs are removed. There is an improvement of approximately 2% accuracy with IHR-Densenet121. For each model, there is an increase in training and validation loss when the lesion is obstructed with hair.

Figure. 6 shows a comparison of improvement in training accuracy and loss after dehairing.

The training accuracy and loss curves are drawn and contrasted for both hair and dehair datasets. It is seen that accuracy and loss curves after dehairing with the proposed IHR models are better and show improved results than with hair.

3.3. Experimental Results with Noise Dataset

The model performance for Noise Dataset is shown in Tables 10-13. Table 10 shows training and validation accuracy on Noise Occluded images. Table 11 shows training and validation loss on Noise Occluded images. Dense-Net121 achieves highest training accuracy of 96.04% and validation accuracy of 86.50%. VGG19 with occluded noise gives a training accuracy of 78.25 and a validation accuracy of 76.75%.

Denoising Results using Proposed Integrated CNN with Non-Local means Denoising

Denoising is performed using Algorithm 4 proposed in Section 2.2. Table 12 shows training and validation accuracy after Denoising. Table 13 shows training and validation loss after Denoising. It can be seen that training and validation accuracy decreases when the skin image is distorted with noise. DenseNet121 gives training accuracy of 96.04% with noise and 97.45% with INR-DensetNet121 when noise is removed.

The validation accuracy with Densenet121 is 86.50% when noise is present while INR-DenseNet121 gives 87.58% when noise is removed. There is an improvement of approximately 1% in accuracy with INR-Densenet121. For each model, there is an increase in training and validation loss when the lesion is obstructed with noise.

Figure. 7 shows a comparison of improvement in training accuracy and loss after denoising. The training accuracy and loss curves are drawn and contrasted for both noise and denoise datasets. It is seen that INR models give more accurate output. The accuracy and loss curves after denoising are better and show improved results than with noise.

3.4. Comparison of Ground Truth with Hair, Noise, Dehairing and Denoising

Extensive experimentation is performed to analyze the distortions' effect on the overall diagnosis of skin lesions. Here, comparison graphs are drawn that compare ground truth results with the occluded dataset (Hair Dataset and Noise Dataset) and refined dataset (dehairing and denoising). Figure. 8 shows a comparison between training and validation accuracy for ground truth, hair and dehair images. Figure. 9 shows a comparison between training and validation loss for ground truth, hair and dehair images.

The proposed IHR model is employed for dehairing. Figure. 10 shows a comparison between training and validation accuracy for ground truth, noised, and denoised images. Figure.11 shows a comparison between training and validation loss for ground truth, noised, and denoised images. The proposed INR model is employed for denoising.

From Figure. 10-13, it can be interpreted that the proposed IHR-DenseNet121 achieves 2.3% higher accuracy than DenseNet121 with hair occlusion and the proposed INR-DenseNet121 achieves 1.41% higher accuracy than DenseNet121 with noise occlusion.

It can be interpreted from the results that these appearances often result in low accuracy and high loss in skin lesion classification. The comparison of the results computed by deep learning models with and without artefacts has exposed a significant difference in employing a method for restoring distorted parts.

4. Discussion

4.1. Performance Comparison with Existing Methods

The performance of the proposed hair removal method is compared with published hair detection and segmentation algorithms. Table 14 shows the accuracy metric computed for all algorithms in the presence of hair and after dehairing. The proposed noise removal is compared with available methods for denoising. Table 15 shows the accuracy metric computed for all algorithms after denoising.

Table 14 and Table 15 show that the proposed methods achieve comparable results to existing computer vision techniques. The proposed IHR-DenseNet121, IHR-ResNet50 and IHR-ResNet152 outperform existing methods in dehairing. INR-DenseNet121, INR-ResNet50 and INR-VGG19 models for noise removal beat available methods in the literature. The proposed methods can remove partial occlusion causing elements with more accuracy and perform precise classification of lesions according to class.

In this work, the effects of skin images occluded with hair and noise are analyzed. Components, such as hair and noise, affect image quality and cause classification inaccuracies. These artefacts disrupt the features that get occluded behind them. If a lesion feature is not accurately determined, the diagnosis may not be appropriate. Therefore, it is necessary to diminish the effect of such elements.

This is the first work where 5000 images are adulterated with hair and noise. The projected model can successfully eliminate the effects of occluded regions thereby resulting in better precision. Skin lesions bounded by these undesirable artefacts such as hair and noise are successfully corrected and classified with the inclusion of IHR and INR models with Inpainting and Non-Local Means, respectively. These methods mask any hair and noise hiding the lesion part and preserve the features occluded by them. The examination of results after applying these methods has shown that the integrated models are capable of effectively classifying skin lesions regardless of the presence of unwanted artefacts. This automatic and efficient CAD system can help in the robust analysis of skin lesions in dermoscopic images saving doctors and patients' time.

5. Conclusion

Skin lesion images suffer from artefacts like hairy pixels, noise, poor color contrast, low illumination, moles, bubbles, resolution, etc. In this work, datasets are created with hair and noise to make this CAD system fit in a more realistic scenario. The hairy strands in skin lesion images add extra features that can lead to misdiagnosis. Noise artefacts diminish the visual quality of digital images, lowering the precision and accuracy of image analysis operations. The effect of noise and hair artefacts on diagnostic accuracies is studied here and it is perceived that these artefacts lack accuracy and can be a reason for inaccurate analysis. Noise and hair removal techniques can enhance image quality. Removal and restoration of the regions after hair and noise removal is vital so that features within lesions can be examined more thoroughly and primary stage. It is concluded that the proposed integrated CNN i.e. IHR and INR can do an improved and accurate diagnosis of lesions from dermoscopic images after image restoration. This analysis is crucial to studying unwanted segmentation and classification results of lesion images due to the presence of the hairs and noise covering them. The output of the proposed methods delivers more accurate and quality results. Many other artefacts like ruler marks, color charts, ink marks, moles, a fuzzy border, and numerous shades of color should also be isolated and corrected. There is a necessity for an automatic hair removal method that preserves all the lesion features in the presence of all these artefacts while keeping its computational cost low for accurate melanoma recognition and classification tasks. The future work focuses on developing a deep learning method for image inpainting and restoration.

Acknowledgments

The author would like to express his heartfelt gratitude to the supervisor for his guidance and unwavering support during this research for his guidance and support.

References

1. Esteva A, Kuprel B, Novoa RA, Ko J, Swetter SM, Blau HM, Thrun S. Dermatologist-level classification of skin cancer with deep neural networks. Nature 2017; 542 (7639): 115-118. https://doi.org/10.1038/nature21056

2. Yang DD, Salciccioli JD, Marshall DC, Sheri A, Shalhoub J. Trends in malignant melanoma mortality in 31 countries from 1985 to 2015. British Journal of Dermatology 2020; 183 (6): 1056-1064. https://doi.org/10.1111/bjd.19010

3. Mahbod A, Schaefer G, Wang C, Ecker R, Ellinge I. Skin lesion classification using hybrid deep neural networks. In: ICASSP 2019-2019 IEEE International Conference on Acoustics, Speech and Signal Processing; Brighton, UK, pp. 1229-1233. https://doi.org/10.1109/ICASSP.2019.8683352

4. Conforti C, Giuffrida R, Vezzoni R, Resende FSS, Meo N, Zalaudek I. Dermoscopy and the experienced clinicians. International Journal of Dermatology 2020; 59 (1): 16-22. https://doi.org/10.1111/ijd.14512

5. Yu L, Chen H, Dou Q, Qin J, Heng P-A. Automated melanoma recognition in dermoscopy images via very deep residual networks. IEEE transactions on medical imaging 2017; 36 (4): 994-1004. https://doi.org/10.1109/TMI.2016.2642839

6. Celebi ME, Iyatomi H, Schaefer G, Stoecker WV. Lesion border detection in dermoscopy images. Computerized medical imaging and graphics 2009; 33 (2): 148-153. https://doi.org/10.1016/j.compmedimag.2008.11.002

7. Xie Y, Zhang J, Xia Y, Shen C. A mutual bootstrapping model for automated skin lesion segmentation and classification. IEEE transactions on medical imaging 2020; 39 (7): 2482-2493. https://doi.org/10.1109/TMI.2020.2972964

8. Zhu L, Feng S, Zhu W, Chen X. ASNet: An adaptive scale network for skin lesion segmentation in dermoscopy images. In: Medical Imaging 2020, Biomedical Applications in Molecular, Structural, and Functional Imaging; Houston, Texas, United States, 2020; 11317. https://doi.org/10.1117/12.2549178

9. Li H, He X, Zhou F, Yu Z, Ni D, Chen S, Wang T, Lei B. Dense deconvolutional network for skin lesion segmentation. IEEE journal of biomedical and health informatics 2019; 23 (2): 527-537. https://doi.org/10.1109/JBHI.2018.2859898

10. Lee T, Ng V, Gallagher R, Coldman A, McLean D. Dullrazor: A software approach to hair removal from images. Computers in biology and medicine 1997; 27 (6): 533-543. https://doi.org/10.1016/S0010-4825(97)00020-6

11. Chung DH, Sapiro G. Segmenting skin lesions with partial-differential-equations-based image processing algorithms. IEEE Transactions on Medical Imaging 2000; 19 (7): 763-767. https://doi.org/10.1109/42.875204

12. Zhou H, Chen M, Gass R, Rehg JM, Ferris L, Ho J, Drogowski L. Feature-Preserving Artifact Removal from Dermoscopy Images. In: Medical Imaging, Image Processing, 2008, vol. 6914, pp. 439-447. https://doi.org/10.1117/12.770824

13. Silveira M, Nascimento JC, Marques JS, Marçal AR, Mendonça T, Yamauchi S, Maeda J, Rozeira J. Comparison of segmentation methods for melanoma diagnosis in

dermoscopy images. IEEE Journal of Selected Topics in Signal Processing 2009; 3 (1): 35-45. https://doi.org/10.1109/JSTSP.2008.2011119

14. Xie F, Qin S, Jiang Z, Meng R. PDE-based unsupervised repair of hair-occluded information in dermoscopy images of melanoma. Computerized Medical Imaging and Graphics 2009; 33 (4): 275-282. https://doi.org/10.1016/j.compmedimag.2009.01.003

15. Abbas Q, Celebi ME, García IF. Hair removal methods: a comparative study for dermoscopy images. Biomedical Signal Processing and Control 2011; 6 (4): 395-404. https://doi.org/10.1016/j.bspc.2011.01.003

16. Toossi MTB, Pourreza HR, Zare H, Sigari MH, Layegh P, Azimi A. An effective hair removal algorithm for dermoscopy images. Skin Research and Technology 2013; 19: 230-235. https://doi.org/10.1111/srt.12015

17. Abuzaghleh O, Barkana BD, Faezipour M. Noninvasive real-time automated skin lesion analysis system for melanoma early detection and prevention. IEEE Journal of Translational Engineering in Health and Medicine 2015; 3: 1-12. https://doi.org/ 10.1109/JTEHM.2015.2419612

18. Kasmi R, Mokrani K. Classification of malignant melanoma and benign skin lesions: implementation of automatic ABCD rule. IET Image Processing 2016; 10 (6): 448-455. https://doi.org/10.1049/iet-ipr.2015.0385

19. Shin DH, Park RH, Yang S, Jung JH. Block-based noise estimation using adaptive Gaussian filtering. IEEE Transactions on Consumer Electronics 2005; 51 (1): 218-226. https://doi.org/10.1109/TCE.2005.1405723

20. Leavline EJ, Sutha S. Gaussian noise removal in gray scale images using fast Multiscale Directional Filter Banks. In: Proceedings of the 27th Annual International

Conference on Recent Trends in Information Technology (ICRTIT); Chennai, India, pp. 884-889. https://doi.org/ 10.1109/ICRTIT.2011.5972377

21. Liu W, Lin WS. Additive white Gaussian noise level estimation in SVD domain for images. IEEE Transactions on Image processing 2013; 22 (3): 872-883. https://doi.org/ 10.1109/TIP.2012.2219544

22. Bouboulis P, Slavakis K, Theodoridis S. Adaptive kernel-based image denoising employing semi-parametric regularization. IEEE Trans Image Process 2010; 19 (6): 1465-1479. https://doi.org/10.1109/TIP.2010.2042995

23. Beck A, Teboulle M. Fast gradient-based algorithms for constrained total variation image denoising and deblurring problems. IEEE transactions on image processing 2009; 18 (11): 2419-2434. https://doi.org/10.1109/TIP.2009.2028250

24. Zhang L, Dong WS, Zhang D, Shi GM. Two-stage image denoising by principal component analysis with local pixel grouping. Pattern recognition 2010; 43 (4): 1531-1549. https://doi.org/10.1016/j.patcog.2009.09.023

25. Guo Q, Zhang CM, Zhang YF, Liu H. An efficient SVD-based method for image denoising. IEEE transactions on Circuits and Systems for Video Technology 2016; 26: 868-880. https://doi.org/10.1109/TCSVT.2015.2416631

26. Del Amor R, Morales S, Colomer A, Mogensen M, Jensen M, Israelsen NM, Naranjo V. Automatic segmentation of epidermis and hair follicles in optical coherence tomography images of normal skin by convolutional neural networks. Frontiers in Medicine 2020; 7: 220. https://doi.org/10.3389/fmed.2020.00220

27. Akyel C, Arici N. Hair Removal and Lesion Segmentation with FCN8-ResNetC and Image Processing in Images of Skin Cancer. Bilişim Teknolojileri Dergisi 2022; 15 (2): 231-238. https://doi.org/10.17671/gazibtd.1060330

28. Jain V, Seung S. Natural image denoising with convolutional networks, In Advances in neural information processing systems 2009; 769-776. http://dx.doi.org/10.1109/icip.2019.8803367

29. Xie J, Xu L, Chen E. Image denoising and inpainting with deep neural networks. In Advances in neural information processing systems 2012; 341-349. http://dx.doi.org/10.1016/j.neunet.2019.08.022

30. Mao X, Shen C, Yang YB. Image restoration using very deep convolutional encoder-decoder networks with symmetric skip connections. In Advances in neural information processing systems 2016; 2802-2810. http://dx.doi.org/10.1007/s11760-021-01982-7

31

32. Boyat AK, Joshi BK. A review paper: noise models in digital image processing. arXiv preprint arXiv:1505.03489, 2015

33. https://www.tensorflow.org/datasets/catalog/imagenet2012

34. https://challenge.isic-archive.com/data/#2016

35. He, Kaiming, Xiangyu Zhang, Shaoqing Ren, Jian Sun. Deep residual learning for image recognition. In: Proceedings of the IEEE Conference on Computer Vision and Pattern Recognition 2016; 770-778. http://dx.doi.org/10.1109/cvpr.2016.90

36. https://iq.opengenus.org/architecture-of-densenet121/

37. Simonyan, Karen, Andrew Zisserman, Very deep convolutional networks for large-scale image recognition. http://dx.doi.org/10.1109/cvpr.2016.182

38. https://viso.ai/deep-learning/vgg-very-deep-convolutional-networks/

39. Comer Mary L, Edward J. Delp III. Morphological operations for color image processing. Journal of electronic imaging 1999; 8(3): 279-289. https://doi.org/10.1117/1.482677

40. Sahoo Prasanna K, Soltani SAKC, Andrew Wong KC. A survey of thresholding techniques. Computer vision, graphics, and image processing 1988; 41 (2): 233-260.

41. Telea Alexandru, An image inpainting technique based on the fast-marching method. Journal of Graphics Tools 2004; 9(1): 23-34. https://doi.org/10.1080/10867651.2004.10487596

42. Buades, Antoni, Bartomeu Coll, Jean-Michel Morel. Non-local means denoising. Image Processing on Line 2011; 1: 208-212. https://doi.org/10.5201/ipol.2011.bcm_nlm

43. Agarap Abien Fred. Deep learning using rectified linear units (relu). arXiv preprint arXiv:1803.08375. 2018. https://doi.org/10.48550/arXiv.1803.08375

44. Kingma, Diederik P, Jimmy Ba. Adam: A method for stochastic optimization. arXiv preprint arXiv:1412.6980. 2014. https://doi.org/10.1111/j.1600-0846.2011.00603.x

45. Zhang Z, Sabuncu, M. Generalized cross entropy loss for training deep neural networks with noisy labels. Advances in neural information processing systems 2018; 31. http://dx.doi.org/10.1016/j.neunet.2021.07.024

46. Fiorese M, Peserico E, Silletti A. VirtualShave: automated hair removal from digital dermatoscopic images. In: Proceedings of the Annual International Conference of the IEEE Engineering in Medicine and Biology Society; Boston, MA, USA, pp. 5145-5148. http://dx.doi.org/10.1109/iembs.2011.6091274

47. Huang A, Kwan SY, Chang WY, Liu MY, Chi MH, Chen GS. A robust hair segmentation and removal approach for clinical images of skin lesions. In: Proceedings of the 35th annual international conference of the IEEE engineering in medicine and biology society (EMBC), Osaka, Japan; pp. 3315–3318. https://doi.org/10.1109/EMBC.2013.6610250

48. Abbas IF Garcia M, Emre Celebi, Ahmad W. A feature preserving hair removal algorithm for dermoscopy images, Skin Research and Technology 2013; 19 (1): e27-e36. https://doi.org/10.1111/j.1600-0846.2011.00603

49. Koehoorn J, Sobiecki AC, Boda D, Diaconeasa A, Doshi S, Paisey S, Telea A. Automated digital hair removal by threshold decomposition and morphological analysis. In: Proceedings of the 12th International Symposium Mathematical Morphology and Its Applications to Signal and Image Processing, ISMM; Reykjavik, Iceland, pp. 15-26. https://doi.org/10.1007/ 978-3-319-18720-4_2

50. Lee I, Du X, Anthony B. Hair segmentation using adaptive threshold from edge and branch length measures. Computers in biology and medicine 2017; 89: 314-324. https://doi.org/10. 1016/j.compbiomed.2017.08.020

51. Kasmi R. SharpRazor: automatic removal of hair and ruler marks from dermoscopy images. Skin Research and Technology 2021. https://doi.org/10.1111/srt.13203

52. Ronneberger O, Fischer P, Brox T. U-Net: Convolutional Networks for Biomedical Image Segmentation. In: Proceedings of the Medical Image Computing and Computer-Assisted Intervention MICCAI; Munich, Germany, pp. 5-9. https://doi.org/10.1007/978-3-319-24574-4_28

53. Xiong W, Jia X, Yang D, Ai M, Li L, Wang S. DP-LinkNet: A convolutional network for historical document image binarization. KSII Transactions on Internet and Information Systems (TIIS) 2021; 15: 1778-1797. https://doi.org/10.3837/tiis.2021.05.011

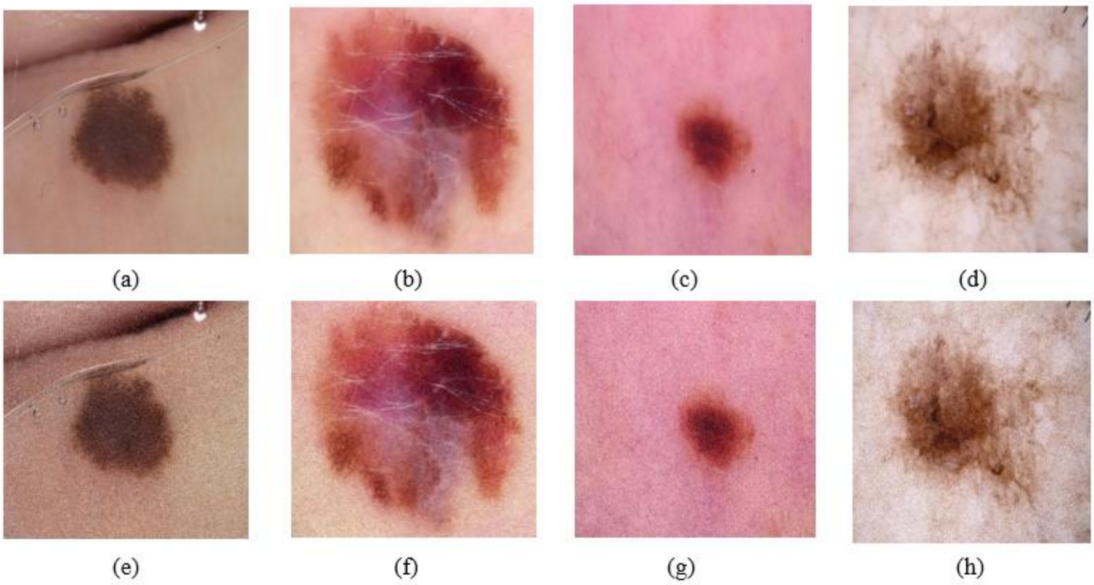

Figure. 1 (a)-(d) are images from original HAM10000 dataset, (e)-(h) are corresponding noise added images

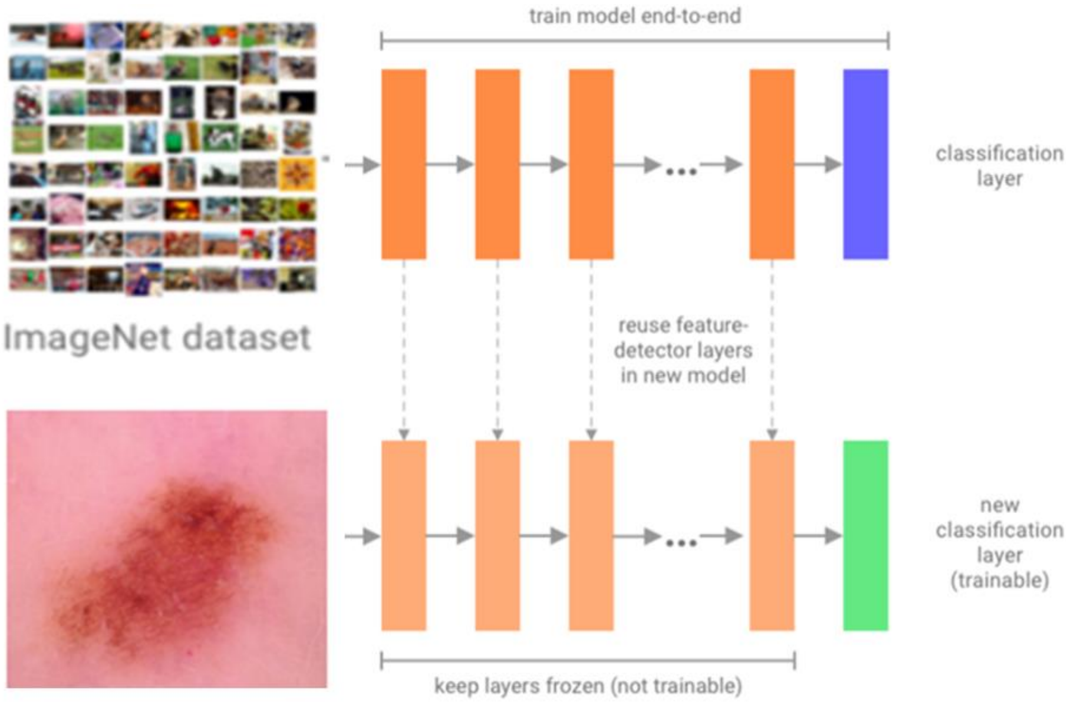

Figure. 2 Proposed CNN for Dermoscopic Images Classification

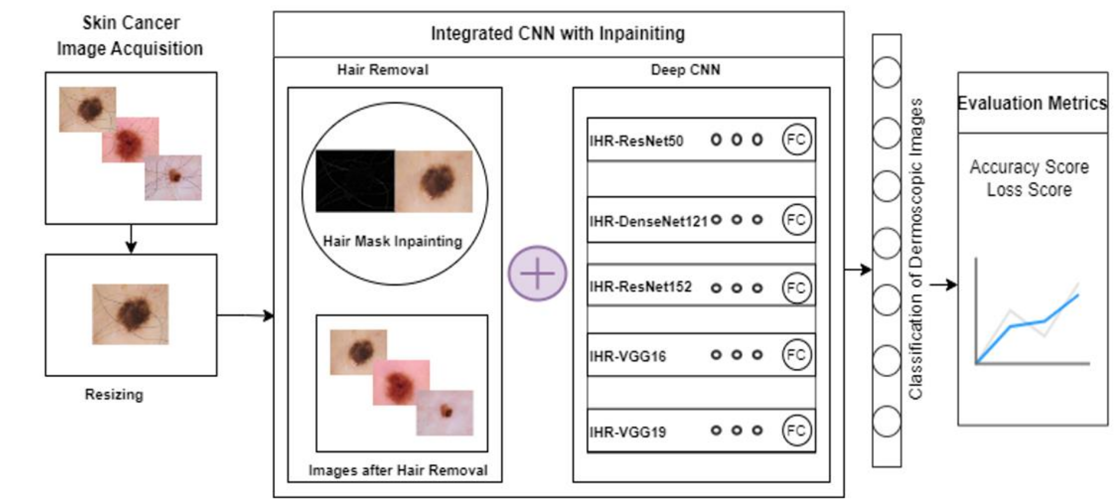

Figure. 3 Integration of CNN with Inpainting for Dermoscopic Hair Removal and Classification

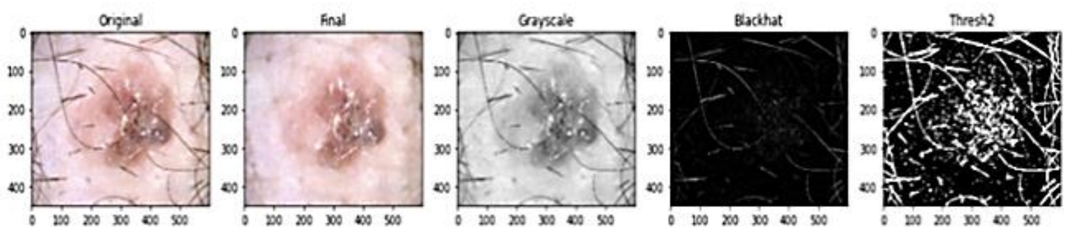

Figure. 4 Stages of the Hair removal process for Dermoscopic images

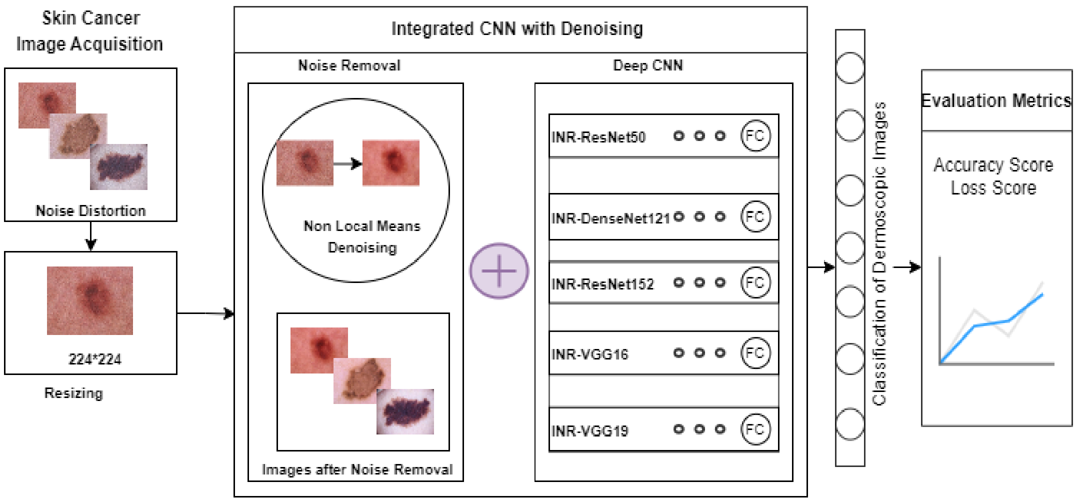

Figure. 5 Integration of CNN with Denoising for Dermoscopic Noise Removal and Classification

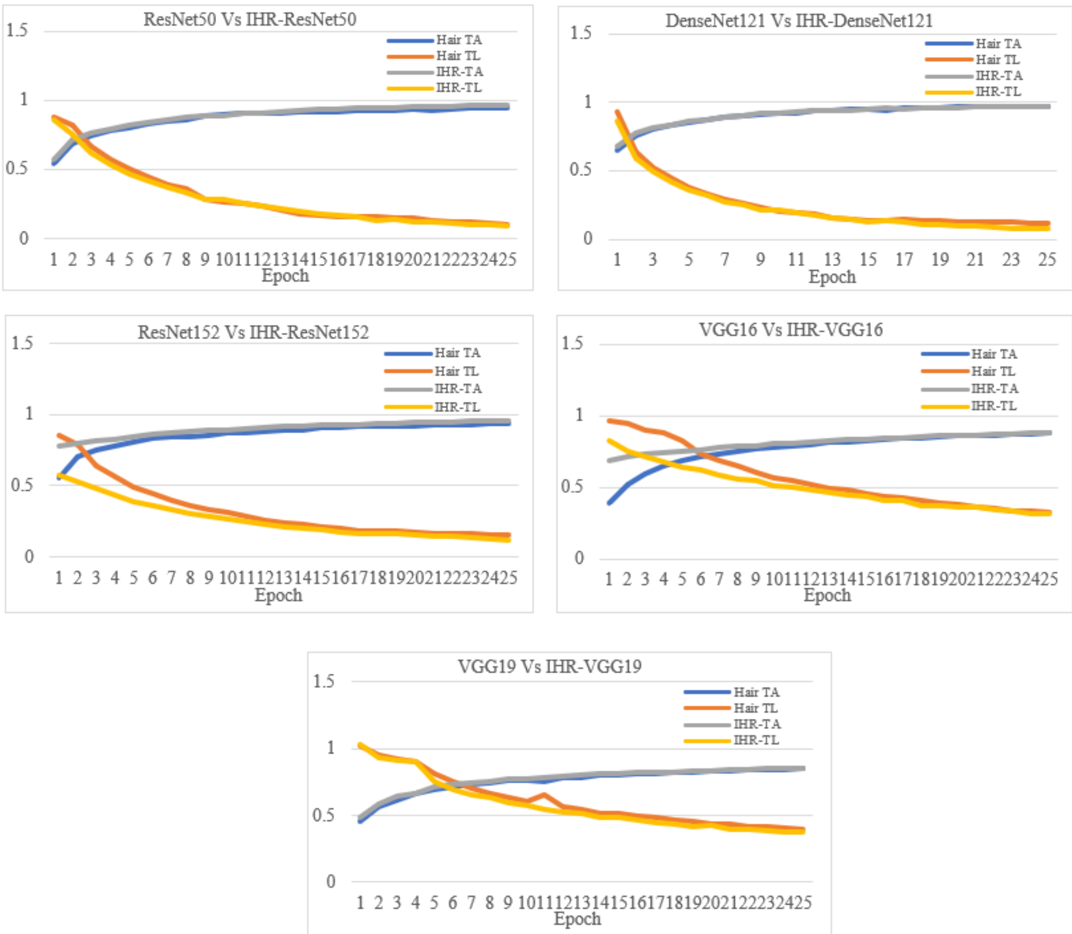

Figure. 6 Comparison of Improvement in Training Accuracy and Loss after Dehairing

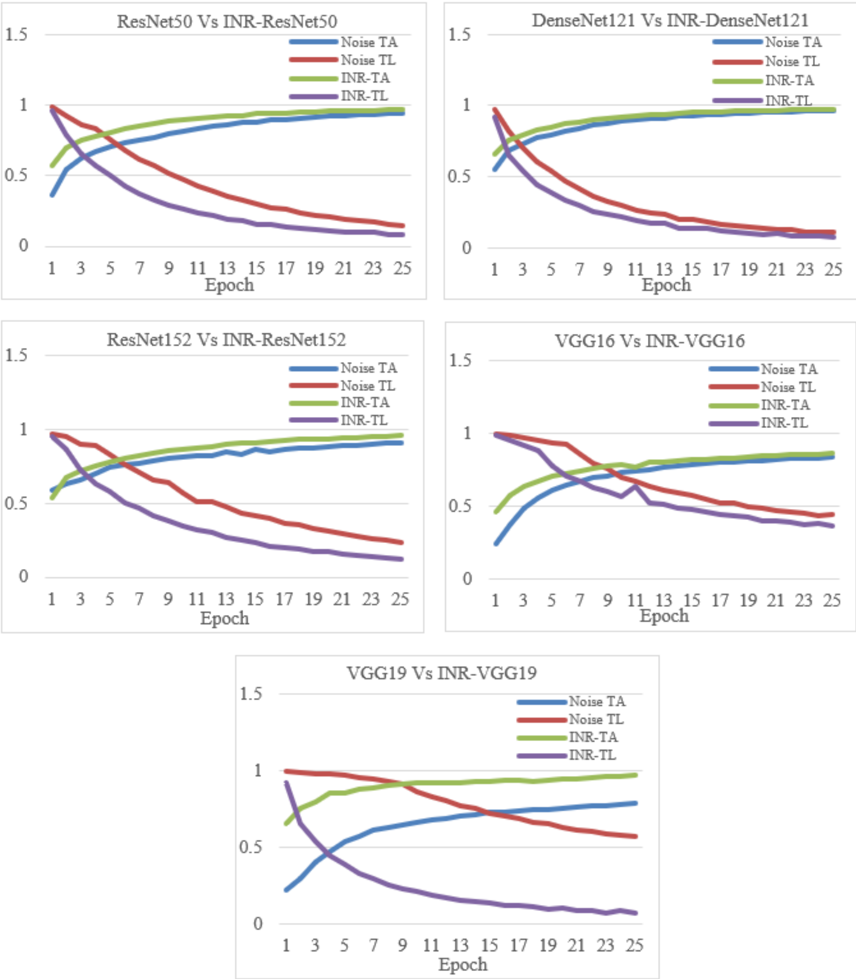

Figure. 7 Comparison of Improvement in Training Accuracy and Loss after Denoising

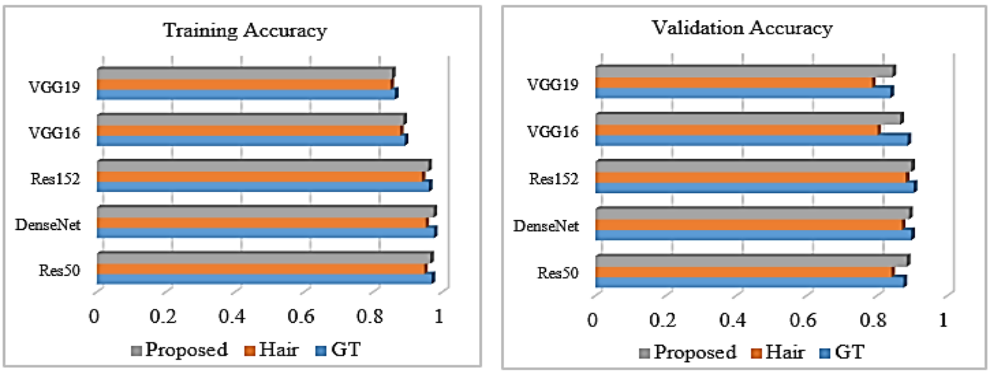

Figure. 8 Comparison of Improvement in Training and Validation Accuracy for GT, Hair, and Proposed IHR Model

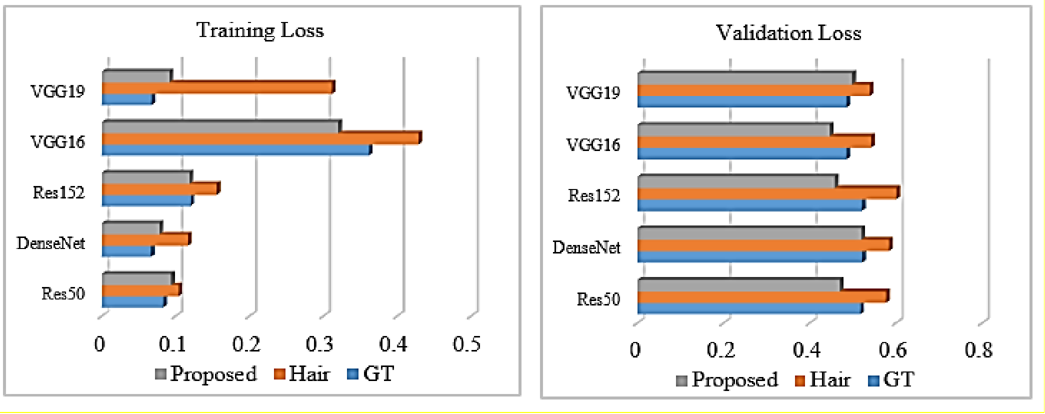

Figure. 9 Comparison of Improvement in Training and Validation Loss for GT, Hair, and Proposed IHR Model

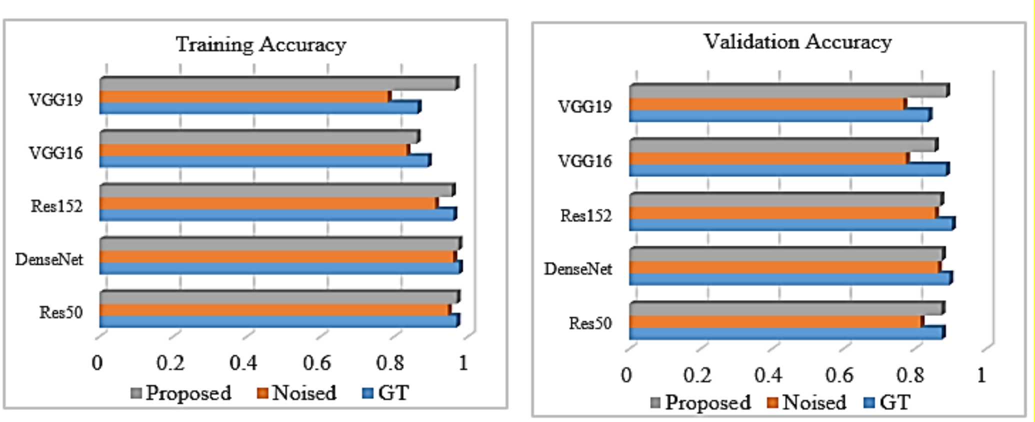

Figure. 10 Comparison of Improvement in Training and Validation Accuracy for GT, Noised, and Proposed INR Model

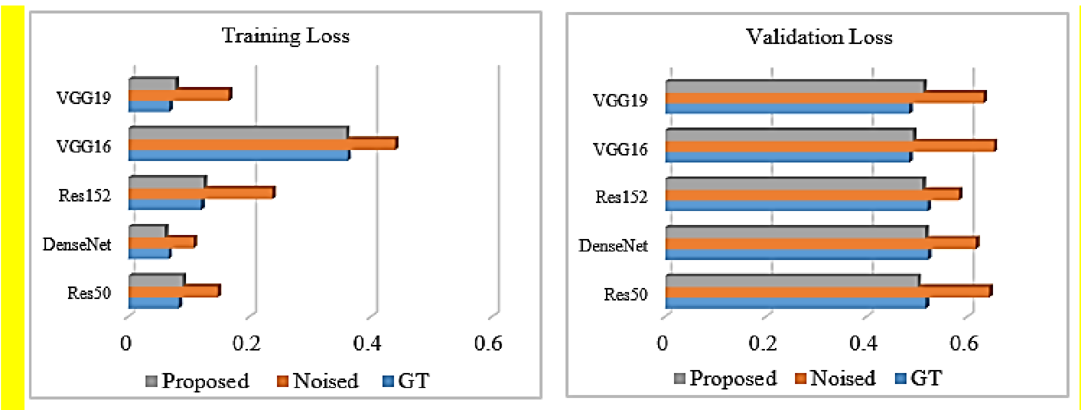

Figure. 11 Comparison of Improvement in Training and Validation Loss for GT, Noised and Proposed INR Model

Table 1. Number of Images per Category in the Dataset

Dataset	Description	No. of images opted for occlusion	No. of images for Classification
Dataset 1	Original Ground truth	-	10015
Dataset 2	Hair Strands	5000	10015
Dataset 3	Noise (Gaussian)	5000	10015

Table 2. Details of Deep Learning Architectures

Features	ResNet50	DenseNet121	ResNet152	VGG16	VGG19
No. of Layers	50	121	152	16	19
Top 5 Accuracy	0.921	0.923	0.931	0.901	0.900
No. of Parameters	25 million	8 million	60 million	138 million	143 million
Size	98 MB	33 MB	232 MB	528 MB	549 MB
Depth	168	121	-	23	26

Table 3. Hyperparameters for the proposed work

S.No.	Name of Hyperparameter	Value of Hyperparameter
1.	Input Size	224 × 224 × 3
2.	Batch Size	32
3.	Epochs	25
4.	Optimization Function	ADAM
5.	Learning Rate	1e-3
6.	Loss function	Categorical Cross entropy
7.	Activation function	ReLU

Table 4. Training and Validation Accuracy on GT Dataset.

Epoch	ResNet50		DenseNet121		ResNet152		VGG16		VGG19	
	TAcc	VAcc	TAcc	VAcc	TAcc	VAcc	TAcc	VAcc	TAcc	VAcc
10	0.9027	0.8407	0.9382	0.8701	0.8921	0.8595	0.8132	0.8210	0.7827	0.8129
15	0.9414	0.8803	0.9569	0.8970	0.9255	0.9004	0.8520	0.8603	0.8230	0.8166
25	0.9694	0.8756	0.9763	0.8972	0.9614	0.9043	0.8918	0.8872	0.8634	0.8380

Table 5. Training and Validation Loss on GT Dataset

Epoch	ResNet50		DenseNet121		ResNet152		VGG16		VGG19	
	TLoss	VLoss	TLoss	VLoss	TLoss	VLoss	TLoss	VLoss	TLoss	VLoss
10	0.2631	0.4683	0.1663	0.4030	0.3471	0.4254	0.5697	0.5685	0.2079	0.5010
15	0.159	0.4446	0.1167	0.5547	0.2351	0.5132	0.4771	0.4619	0.1345	0.4619
25	0.0832	0.5175	0.0665	0.5219	0.1202	0.5213	0.3617	0.4852	0.0675	0.4852

Table 6. Training and Validation Accuracy on Hair Dataset

Epoch	ResNet50		DenseNet121		ResNet152		VGG16		VGG19	
	TAcc	VAcc	TAcc	VAcc	TAcc	VAcc	TAcc	VAcc	TAcc	VAcc
10	0.9001	0.7932	0.9131	0.8283	0.8688	0.8423	0.7811	0.7731	0.7693	0.7273
15	0.9264	0.8129	0.9398	0.8447	0.9096	0.8752	0.8275	0.7922	0.8053	0.7710
25	0.9478	0.8411	0.952	0.8710	0.9412	0.8819	0.8780	0.8018	0.8503	0.7862

Table 7. Training and Validation Loss on Hair Dataset

Epoch	ResNet50		DenseNet121		ResNet152		VGG16		VGG19	
	TLoss	VLoss	TLoss	VLoss	TLoss	VLoss	TLoss	VLoss	TLoss	VLoss
10	0.2609	0.4465	0.204	0.4081	0.3087	0.4290	0.5705	0.5050	0.6049	0.5174
15	0.1688	0.4651	0.1352	0.5044	0.2144	0.4828	0.4538	0.4505	0.513	0.5715
25	0.1038	0.5772	0.1165	0.5837	0.1553	0.6012	0.4287	0.5424	0.3114	0.5390

Table 8. Training and Validation Accuracy after Dehairing on Hair Dataset

Epoch	IHR-ResNet50		IHR-DenseNet121		IHR-ResNet152		IHR-VGG16		IHR-VGG19	
	TAcc	VAcc	TAcc	VAcc	TAcc	VAcc	TAcc	VAcc	TAcc	VAcc
10	0.8918	0.8506	0.9184	0.8556	0.8949	0.8481	0.8134	0.7814	0.7754	0.8534
15	0.9327	0.8738	0.9506	0.8836	0.9288	0.8524	0.8549	0.8179	0.8142	0.8229
25	0.9656	0.8847	0.9750	0.8916	0.9601	0.89	0.8879	0.8663	0.8546	0.8445

Table 9. Training and Validation Loss after Dehairing on Hair Dataset

Epoch	IHR-ResNet50		IHR-DenseNet121		IHR-ResNet152		IHR-VGG16		IHR-VGG19	
	TLoss	VLoss	TLoss	VLoss	TLoss	VLoss	TLoss	VLoss	TLoss	VLoss
10	0.2819	0.4567	0.2122	0.3898	0.2701	0.4991	0.5144	0.5511	0.2788	0.4354
15	0.1810	0.4651	0.1318	0.4114	0.1890	0.4860	0.433	0.5582	0.1861	0.4567
25	0.0938	0.4696	0.0779	0.5198	0.1187	0.4581	0.3202	0.4461	0.0914	0.4985

Table 10. Training and Validation Accuracy on Noise Dataset

Epoch	ResNet50		DenseNet121		ResNet152		VGG16		VGG19	
	TAcc	VAcc	TAcc	VAcc	TAcc	VAcc	TAcc	VAcc	TAcc	VAcc
10	0.8179	0.7791	0.8871	0.8265	0.8120	0.7712	0.7322	0.7873	0.6642	0.7738
15	0.8821	0.8284	0.9275	0.8623	0.8658	0.8200	0.7848	0.7747	0.7251	0.7694
25	0.9462	0.8158	0.9604	0.8650	0.9114	0.8570	0.8339	0.7748	0.7825	0.7675

Table 11. Training and Validation Loss on Noise Dataset

Epoch	ResNet50		DenseNet121		ResNet152		VGG16		VGG19	
	TLoss	VLoss	TLoss	VLoss	TLoss	VLoss	TLoss	VLoss	TLoss	VLoss
10	0.4723	0.6156	0.2975	0.5243	0.5669	0.4925	0.7012	0.5876	0.2613	0.5627
15	0.3038	0.5725	0.1949	0.5104	0.4144	0.5598	0.5709	0.6058	0.2171	0.6096
25	0.1475	0.6439	0.1078	0.6173	0.2378	0.5835	0.4398	0.6532	0.1656	0.6328

Table 12. Training and Validation Accuracy after Denoising on Noise Dataset

Epoch	INR-ResNet50		INR-DenseNet121		INR-ResNet152		INR-VGG16		INR-VGG19	
	TAcc	VAcc	TAcc	VAcc	TAcc	VAcc	TAcc	VAcc	TAcc	VAcc
10	0.8982	0.8525	0.9179	0.8883	0.8672	0.8470	0.7824	0.7744	0.9194	0.8695
15	0.9404	0.8713	0.9505	0.8453	0.9080	0.8425	0.8169	0.8373	0.9272	0.8731
25	0.9701	0.8747	0.9745	0.8758	0.9565	0.8710	0.8617	0.8560	0.9665	0.8882

Table 13. Training and Validation Loss after Denoising on Noise Dataset

Epoch	INR-ResNet50		INR-DenseNet121		INR-ResNet152		INR-VGG16		INR-VGG19	
	TLoss	VLoss	TLoss	VLoss	TLoss	VLoss	TLoss	VLoss	TLoss	VLoss
10	0.2631	0.4683	0.2178	0.4030	0.3471	0.4254	0.5697	0.5685	0.2079	0.5010
15	0.159	0.4446	0.1338	0.5547	0.2351	0.5332	0.4771	0.4619	0.1345	0.5318
25	0.0895	0.5015	0.0602	0.5167	0.1242	0.5113	0.3592	0.4922	0.0775	0.5130

Table 14. Comparison with Existing Hair Removal Methods

Year	Method Used	Accuracy with Hair Occlusion	Accuracy Post Hair Removal
(1997) [10]	DullRazor	-	93.15
(2011) [46]	PDE	-	91.74
(2013) [47]	Curvilinear Matched Filtering	-	81.13
(2013) [48]	Derivative of Gaussians	-	87.36
(2015) [49]	Threshold Decomposition	-	80.13
(2017) [50]	ED+MBL	-	90.99

(2021) [51]	SharpRazor	-	93.80
Proposed INR	Inpainting + DenseNet121	95.2	**97.50**
	Inpainting + ResNet50	94.78	**96.56**
	Inpainting + ResNet152	94.12	**96.01**

Table 15. Comparison with Existing Noise Removal Methods

Year	Method Used	Accuracy with Noise Occlusion	Accuracy Post Noise Removal
(2016) [52]	UNet	-	**87.25**
(2021) [53]	DP-LinkNet	-	**94.86**
Proposed INR	Non-Local Means +DenseNet121	96.04	**97.45**
	Non-Local Means + ResNet 50	94.62	**97.01**
	Non-Local Means + VGG19	78.25	**96.65**